Exp Fluids (2010) 49:355–365
DOI 10.1007/s00348-009-0764-9

RESEARCH ARTICLE

Behavior of shock trains in a diverging duct

A. Weiss · A. Grzona · H. Olivier

Received: 11 May 2009 / Revised: 26 September 2009 / Accepted: 28 September 2009 / Published online: 6 January 2010

Abstract A shock train inside a diverging duct is analyzed at different pressure levels and Mach numbers. Nonreactive pressurized cold gas is used as fluid. The structure and pressure recovery inside the shock train is analyzed by means of wall pressure measurements, Schlieren images and total pressure probes. During the course of the experiments, the total pressure of the flow, the back pressure level and the Mach number upstream of the compression region have been varied. It is shown that the Reynolds number has some small effect on the shock position and length of the shock train. However, more dominant is the effect of the confinement level and Mach number. The results are compared with analytical and empirical models from the literature. It was found that the empirical pseudo-shock model from Billig and the analytical mass averaging model from Matsuo are suitable to compute the pressure gradient along the shock train and total pressure loss, respectively.

List of symbols

a	Speed of sound (m/s)
c	Empirical constant 0.114
D	Diameter or equivalent diameter of the duct (m)
H	Duct height (m)
L_p	Length of the pseudo-shock (m)
Ma	Mach number
Ma′	Mean Mach number of the core flow
Ma″	Mean Mach number of subsonic outer region
$\bar{\mathrm{M}}\mathrm{a}_1$	Mass averaged upstream Mach number
$\dot{m}$	Mass flow (kg/s)
n	Experimentally determined constant $n = 2.2$
p_0	Total pressure in the settling chamber (bar)
p/p_1	Ratio of local wall pressure to upstream static pressure
Re_x	Reynolds number based on the distance from the nozzle throat
Re*	Reynolds number based on throat height
Re_θ	Reynolds number based on boundary layer momentum thickness
T_o	Total temperature in the settling chamber (K)
u	Flow velocity (m/s)
w^*	Crocco number at sonic conditions $w^* = \sqrt{(\gamma-1)/(\gamma+1)}$
w'	Crocco number in the isentropic core $w' = u/\sqrt{2c_pT_o}$
$w_{1,2}$	Crocco number upstream/downstream of pressure rise $w_{1,2} = u_{1,2}/\sqrt{2c_pT_o}$
x	Distance downstream from the beginning of the pressure rise (m)

Greek symbols

$\alpha_{1,2,3,4}$	Diverging half-angle of Laval nozzle (°)
δ	Boundary layer thickness (mm)
δ^*	Boundary layer displacement thickness (mm)
θ	Boundary layer momentum thickness for undisturbed flow (mm)
γ	Isentropic exponent
σ	Correction factor for the mass averaging pseudo-shock model
ξ	Correction factor for the mass averaging pseudo-shock model
ρ	Density (kg/m^3)
μ	Mass flow ratio between boundary layer and core flow

A. Weiss (✉) · A. Grzona · H. Olivier
Shock Wave Laboratory, RWTH Aachen University,
v52056 Aachen, Germany
e-mail: weiss@swl.rwth-aachen.de
URL: www.swl.rwth-aachen.de

Subscripts

1 Flow condition upstream of the shock system
2 Flow conditions downstream of the shock system
e Free stream or edge of boundary layer

1 Introduction

The recompression of supersonic gas flow is a very common flow phenomenon in modern aerodynamics and occurs in a great number of applications for instance supersonic ramjet or scramjet inlets, internal diffusers and supersonic ejectors. Yet the actual mechanism of recompression can be very different. All of them coincide with compression shocks and shock boundary layer interaction.

Under certain conditions even one or more shocks can appear downstream of the first shock. This series of shocks is a so-called 'shock train'. In contrast to other shock systems, the supersonic flow is decelerated at first through a shock system and followed by a mixing region as shown in Fig. 1. Throughout the shock train region, the flow outside the boundary layer remains supersonic, because only at the center line region, the shocks are strong enough to decelerate the flow below Ma = 1. Therefore, the flow undergoes successive changes form supersonic to subsonic. In the mixing region, the flow consists of a double tong like supersonic flow near the center line and a subsonic outer region. However, the supersonic flow does not exhibit any compression shocks. In the mixing region, the transition from supersonic to subsonic conditions is more gradual. For the whole interaction region, Crocco (1958) have coined the term 'pseudo-shock'. To distinguish the actual shock train from the mixing region is not simple. For instance, wall pressure measurements do not exhibit significant changes between the two regions. However, by optical means e.g. a Schlieren system the shock train becomes visible as well as the downstream mixing region (see e.g. Fig. 11).

The occurrence of shock trains is a strong function of the upstream Mach number and the boundary layer thickness. Low Mach numbers Ma < 1.3 and thin boundary layers promote the formation of single normal shocks a so-called normal shock stem. In case of higher Mach numbers, the shock boundary layer interaction becomes stronger and several shocks occur.

The influence of the boundary layer on the shape of the shock train is also referred to as 'flow confinement' effect, which characterizes the ratio of the undisturbed boundary layer thickness δ to the radius or half-height of the duct H. Carroll et al. (1993) have demonstrated this effect in a square duct with a flow Mach number of Ma = 1.6 and a Reynolds number of $Re = 3 \times 10^6$. As shown in Fig. 2, the length of the shock train increases significantly as the confinement level increases. The number of shocks is larger as is the distance between each successive shock, hence the overall length of the shock train increases accordingly.

Also depicted in Fig. 2 is the fact that for a moderate shock boundary layer interaction the Mach stem of the first shock is clearly visible. This kind of shock system is often referred to as λ-shaped. As the confinement effect becomes stronger, this Mach stem disappears and the first shock consists out of two oblique shocks that intersect at the center line of the channel. This type of shock train is referred to as x-shaped.

The influence of the confinement level was also confirmed by Om et al. (1985a) who observed multiple shock interaction and an increase in the overall length of interaction if the confinement was increased but the Reynolds number and Mach number were kept constant.

Figure 3 is a good example for a flow case where the confinement level is sufficiently small to avoid the occurrence of a shock train. Even at comparably high Mach numbers e.g. Ma = 1.8 no shock system occurs but a single normal shock with a lambda foot extends almost across the entire height of the test section.

1.1 Pressure recovery across the pseudo-shock

In a classical pseudo-shock system inside a square duct the pressure recovery across a shock train can be separated in two sections. The pressure rises across the shock train itself followed by the pressure recovery in the mixing region. In the shock train region, the pressure rises rather rapidly and more gradually in the mixing region. The pressure rise in the mixing region is driven by mixing of the supersonic layer with the surrounding subsonic flow. At some point

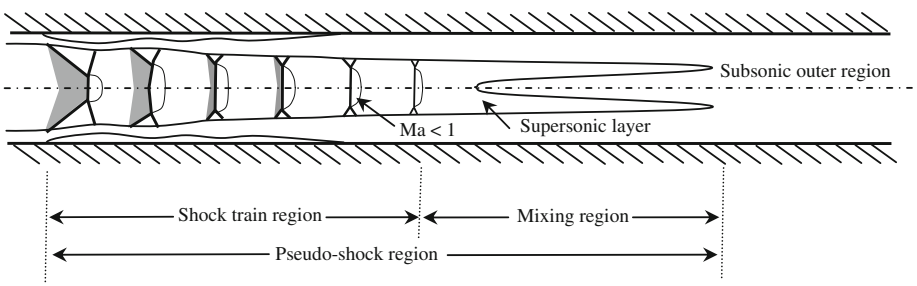

Fig. 1 Sketch of a pseudo-shock system

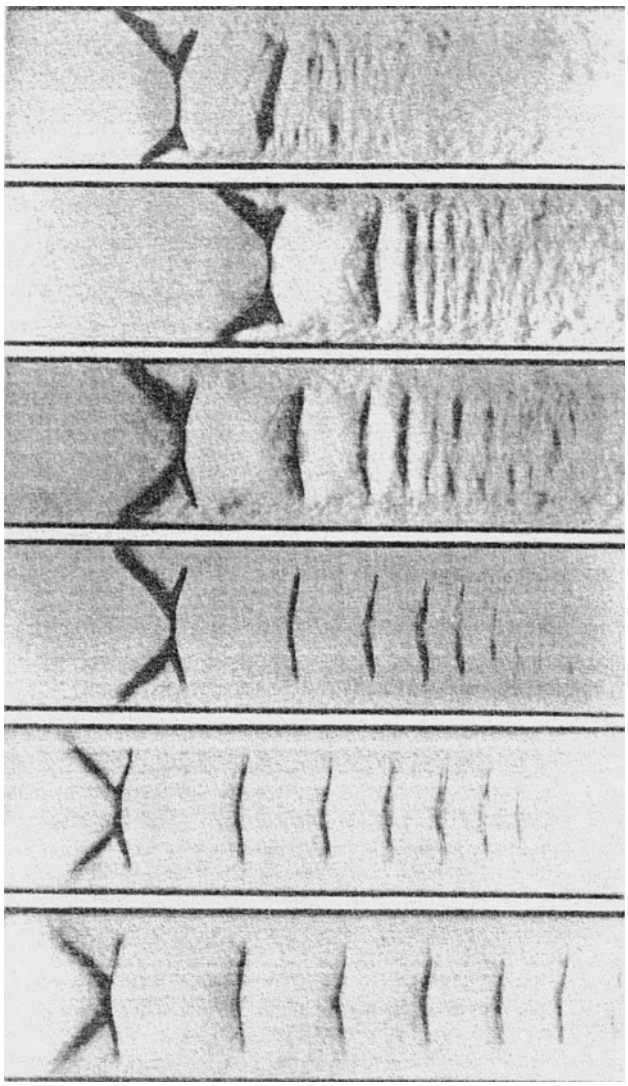

Fig. 2 Shock train as function of confinement effect; Ma = 1.6, δ/H = 0.08, 0.14, 0.27, 0.32, 0.4, 0.49 (Carroll 1990)

downstream the pressure begins to decrease again because pressure losses due to friction exceed the pressure gain due to mixing. This point can also be used as reference point for the length of the pseudo-shock (Crocco 1958).

Waltrup and Billig (1973) quote work from Neumann and Lustwerk (1949) that the pressure rise inside a supersonic wind tunnel diffuser with multiple shocks is near to that of a single normal shock if the boundary layer thickness is reasonably small. This finding is very plausible because in that case most parts of the flow field are compressed by a strong normal shock very similarly to the flow depicted in Fig. 3.

The overall pressure recovery along the shock train is smaller compared to the pressure ratio across a single normal shock wave at the same Mach number because each shock causes a significant total pressure loss (Lukasiewicz 1953). By analyzing a great number of different

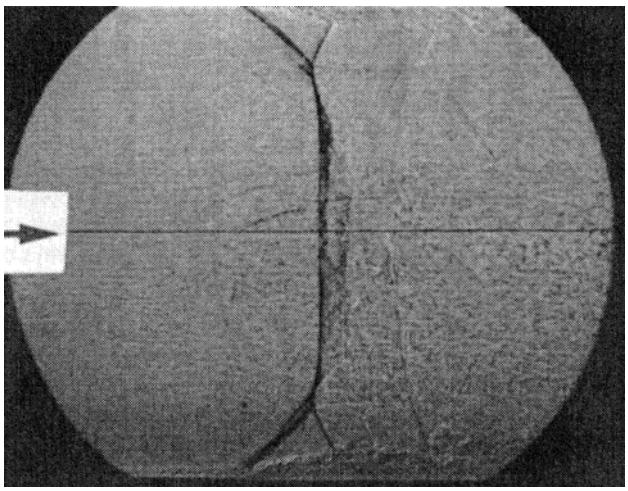

Fig. 3 Spark shadowgraph of a single shock/boundary layer interaction, Ma = 1.8 (Squire 1996)

experiments, Matsuo et al. (1999) have shown that as the shock train length the pressure recovery is not only a function of the Mach number but must also be correlated with the boundary layer thickness, wall friction and turbulence mixing loss.

The presence of multiple shock waves cannot be detected from the wall pressure distribution, because the pressure peaks induced by each shock front are smeared out due to the dissipative character of the boundary layer. Only, flow field measurements of the static or total pressure can resolve the existence of the multiple shock waves. Several researches have carried out measurements of this kind e.g. (Om et al. 1985b; Waltrup and Billig 1973; Cuffel and Back 1976; Matsuo et al. 1990).

This article focuses on the flow characteristics of a shock train, which is placed inside a square channel with diverging upper and lower walls. Due to the very long and slender nozzle shape, the confinement level is very high. The influence of the total pressure on the shock position and length will be discussed as well as the Mach number effect. Analytical models for the length of the shock train and pressure recovery are applied to the shock train at hand and evaluated.

1.2 Experimental facility

The experiments presented in this paper have been carried out in a shock wave reactor. This facility is specifically designed to generate a stable shock train. Initially, the free stream Mach number was conceived to Ma = 1.7 yet as explained later in detail in Sect. 3 the actual free stream Mach number upstream of the shock train was Ma = 1.5. The distance between the nozzle throat and the compression region is 160 mm because the shock system is to be

used to ignite combustible gas, which for that purpose is injected at the nozzle throat (Grzona et al. 2007). However, all experiments presented in this work have been carried out with cold gas. A sketch of the test facility is shown in Fig. 4. The reactor consists of two supersonic nozzles, whereby the first, planar nozzle generates the supersonic flow, therewith the shock train to be investigated and the second, conical nozzle acts as a throttle to adapt the back pressure. Upstream of the primary nozzle, a settling chamber is placed to calm the incoming gas flow. A Venturi nozzle is utilized to measure the volume flow rate from which the mass flow can be calculated. Downstream of the first nozzle, a subsonic diffuser and a square duct are placed. The square duct acts as a settling chamber, which feeds the second nozzle. In order to alternate the back pressure inside the reactor, the throat area of the second nozzle is adjustable by a movable central plug.

Inside the first nozzle both side walls are made from highly transparent quartz glass to allow full optical access. As test gas pressurized air is used that is supplied from a standard compressor. Before the gas enters the settling chamber the humidity is minimized by means of silica gel filters. This is particularly important to avoid any condensation inside the measurements section because the total gas temperature cannot be increased. The maximum mass flow provided by the supply system is $\dot{m} = 0.1$ kg/s. Due to the fixed cross section of the first nozzle throat the total pressure in the reservoir chamber settles at $p_0 = 4.8$ bar when the facility operates at full power.

Despite the fact that a square duct tends to show three dimensional effects for shock boundary layer interaction, it was preferred over an axisymmetric configuration in order to allow optical investigations of the measurement section.

Downstream the nozzle throat the cross section increases in order to obtain a Mach number of Ma = 1.25 followed by a quasi parallel section with a diverging half-angle of only $\alpha_3 = 0.3°$. This was deemed to account for the boundary layer growth, thereby minimizing the pressure gradient in flow direction. As shown in Fig. 5 along the diverging Sect. 160 mm downstream of the nozzle throat the upper and lower wall of the nozzle is tilted by $\alpha_4 = 1.5°$. The wall angle in the compression region is increased in order to stabilize the shock system i.e. the position of the shock, owing to a larger pressure gradient. On the other hand, it is limited to this value to avoid boundary layer separation. The width of the nozzle is 15 mm and the height of the throat 6 mm. A more detailed description of the shock wave reactor can be found in (Grzona et al. 2007).

1.3 Measurement system

The flow inside the diverging section is investigated by means of a boundary layer pressure probe, wall pressure taps and Schlieren images. The boundary layer probe consists of a single, in vertical and horizontal direction movable tube with an outer diameter of 0.9 mm and a wall thickness of 0.1 mm. The tip of the probe is flattened out in order to increase its vertical resolution. The height of the opening of the probe is 0.025 mm, the overall height of the tip is 0.225 mm and its width amounts to 1.1 mm. At the position of the probe tip ($x = 170$ mm), the cross section of the tunnel is 8.2 × 15 mm, therefore the probe covers between 1.75 and 4.75% of the tunnel cross section.

This tube is connected to a pressure scanner, which allows to record up to 16 channels in parallel. Due to velocity fluctuations in the boundary layer, about 100 samples have been recorded at 5 Hz and later averaged. In case of

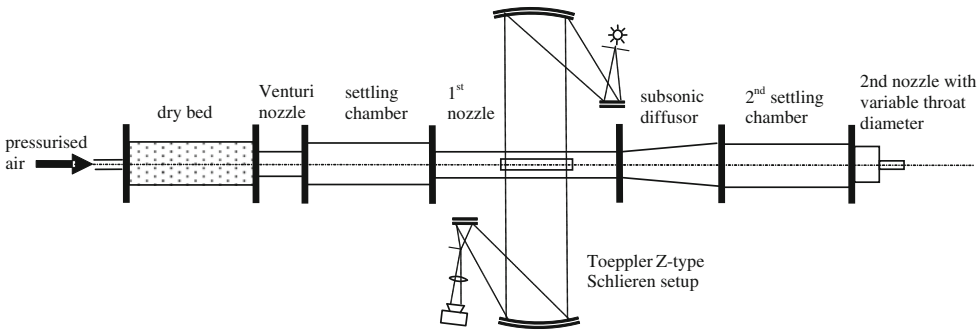

Fig. 4 Schematic sketch of the test facility with Schlieren system

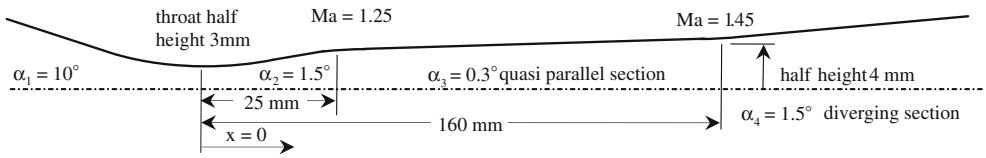

Fig. 5 Sketch of the nozzle contour

measurements inside the supersonic boundary layer a pressure scanner with a pressure range up to 17 bar is utilized. Because of the large difference between the total and static pressure, both values have been measured separately.

The same measurement setup is also used to measure the wall pressure. For that purpose 0.5 mm pressure taps are placed along the center line of the upper and lower nozzle wall. After calibrating the system, the measurement uncertainty was determined with 0.015%, which equals to 2.55 mbar at the upper limit of the measurement range.

As depicted in Fig. 4, a Toepler Z-type Schlieren system is used to study the flow field inside the first nozzle. A flash gun with 10 μs pulse width is used to illuminate the flow field. All Schlieren images shown have been obtained with a vertical knife edge. Expansion waves appear dark whereas compression areas are depicted white.

2 Review of shock train models

Om et al. (1985a) brought forward a one dimensional flow model regarding the formation of a series of normal shocks at Mach 1.6 and a blockage or confinement level of 2.27%, e.g. (area ratio of boundary displacement thickness and geometric cross section). From their measurements they concluded that due to the first shock the displacement thickness of the boundary layer builds up sufficiently to choke the flow. Therefore, the flow accelerates again until supersonic speed is reached, resulting in a second normal shock. Though this model appears to be reasonable, it can only be applied to so-called normal shock trains. Only, when the confinement level is small, and the Mach number is moderate normal shocks occur. Otherwise, as explicated before a lambda or x-shape shock system occurs.

Waltrup and Billig (1973) presented an empirical relationship (1) for the pressure distribution $p(x)$ in the shock train region. This equation was derived from experiments in a constant area duct. In the course of these experiments, the length of the duct has been varied, the Mach number was in the range of Ma = 1.53–2.72, the total pressure hence the Reynolds number and back pressure have also been varied. In a first step the pressure ratio across the shock train was plotted over the length of the shock train. For a constant pressure ratio and Mach number Ma_1, the length of the interaction increases directly with the boundary layer momentum thickness θ_1. The reverse trend holds true for an increased Reynolds number Re_θ, because the oncoming boundary layer is thinner. Also, the results of Waltrup and Billig show that for a fixed shock train length the pressure ratio increases in accordance with the Mach number. Waltrup and Billig suggest that this effect can be attributed to flow separation at the onset of the compression region, which causes stronger shocks and therefore higher pressure gradients.

$$\frac{x\left(\mathrm{Ma}_1^2-1\right)\mathrm{Re}_\theta^{1/4}}{D^{1/2}\theta_1^{1/2}}=50\left(\frac{p}{p_1}-1\right)+170\left(\frac{p}{p_1}-1\right)^2 \quad (1)$$

The empirical Eq. 1 was found to agree well with results obtained by Bement et al. (1990), Nill and Mattick (1996) and Cuffel and Back (1976).

Initially, the above equation was derived from experiments with circular ducts; therefore Billig (1992) has adapted the empirical model also for square ducts given in Eq. 2.

$$\frac{x\left(\mathrm{Ma}_1^2-1\right)\mathrm{Re}_\theta^{1/5}}{H^{1/2}\theta_1^{1/2}}=50\left(\frac{p}{p_1}-1\right)+170\left(\frac{p}{p_1}-1\right)^2 \quad (2)$$

Crocco (1958) was the first author to suggest a model that analytically describes the recompression by a shock train. He assumed that the overall pressure ratio across the shock train is equal to that of a normal shock. However, the dissipative phenomenon of the shock train was considered to reside not in the shocks but in the turbulent dissipation region near the wall while neglecting wall friction. Starting from the initial cross section, where the flow is still undisturbed and supersonic the dissipative region spreads through the isentropic core region. Neglecting any shocks, this model is often termed shock-less model. Unfortunately, the model does not provide any conclusions about the length of the shock train. The pressure along the shock train for the dissipative as well as the core region is considered the same and determined by the following equation, which is only a different representation of the isentropic equation.

$$\frac{p}{p_1}=\left(\frac{1-w^2}{1-w_1^2}\right)^{\gamma/(\gamma-1)} \quad (3)$$

Equation 3 in combination with the conservation equations of mass, energy and momentum can be used to calculate the flow properties across the shock system. However, the computed static pressure rise and total pressure loss across the shock train are equal to those derived from the normal shock equations. This very much overestimates the pressure level observed in the experiments.

Because Croccos shock-less model exhibits some shortcomings in predicting the pressure ratio across the pseudo-shock and also does not yield any pressure distribution along the shock train, a diffusion model has been developed by Ikui et al. (1974). This model takes into account that the core region of the flow is not isentropic. Furthermore, the length of the shock train is defined by the distance where the velocity in the central core region becomes equal to the velocity in the outer dissipative region. These assumptions allow expressing the length of

the shock train as a function of the Crocco number at sonic conditions up- and downstream of the shock train in relation to the critical Crocco number in the nozzle throat and the diameter of the duct (see Eq. 4),

$$\frac{L_p}{D} = \frac{2}{c}\sinh^{-1}\left(\frac{w_1 - w_2}{2w^*}\right) \tag{4}$$

with c being an empirical constant of 0.114. Ikui et al. (1974) evaluated this equation against an equation based on experimental data (NAVWEPS 1959), which is given in Eq. 5. Both equations perform similarly.

$$\frac{L_p}{D} = 18.75\left(1 - \frac{1}{\mathrm{Ma}_1}\right) \tag{5}$$

The static pressure within the pseudo-shock can be computed based on an empirical diffusion equation for the flow velocity in the core flow and the conservation laws of mass, momentum and energy, which leads to Eq. 6.

$$\frac{p - p_1}{p_2 - p_1} = \frac{\left\{w_1^2\left(w_1^2 - 2w^{*2}\right) + w_1^2 w^{*2} e^{-c(x/D)}\right\}\left(1 - e^{-c(x/D)}\right)}{\left(w_1^2 - w^{*2}\right)^2 - w_1^2\left(w_1^2 - w^{*2}\right)\, e^{-c(x/D)}\,\left(1 - e^{-c(x/D)}\right)} \tag{6}$$

Based on their earlier work Ikui et al. (1981) have also developed a modified diffusion model, which considers the upstream turbulent boundary layer and associated friction losses. For that model the equation for the length of the shock train had to be reviewed. This new Eq. 7 has been obtained from experimental data,

$$\frac{L_p}{D} = 3700(\mathrm{Ma}_1' - 1)^{3.8}\mu_1 \tag{7}$$

whereby Ma_1' is the mean upstream Mach number and μ_1 the mass flow ratio of the upstream boundary layer and core flow, respectively. The pressure distribution along the pseudo-shock is described by Eq. 8, where the double primed Mach number is the mean Mach number of the outer subsonic flow region.

$$\frac{p}{p_1} = \left[\frac{(1-\mu)}{\mathrm{Ma}'}\left(1 + \frac{\gamma - 1}{2}\mathrm{Ma}'^2\right)^{-1/2} + \frac{\mu}{\mathrm{Ma}''}\left(1 + \frac{\gamma - 1}{2}\mathrm{Ma}''^2\right)^{-1/2}\right] \Big/ \xi \tag{8}$$

with

$$\xi = \frac{(1-\mu_1)}{\mathrm{Ma}_1'}\left(1 + \frac{\gamma - 1}{2}\mathrm{Ma}_1'^2\right)^{-1/2} + \frac{\mu_1}{\mathrm{Ma}_1''}\left(1 + \frac{\gamma - 1}{2}\mathrm{Ma}_1''^2\right)^{-1/2}$$

Compared to the aforementioned models, the mass averaging pseudo-shock model proposed by Matsuo et al. (1999) is more complex and rather cumbersome to apply. The model applies to pseudo-shocks in a constant area duct with a fully turbulent boundary layer but neglects both friction losses and heat and mass transfer across the wall. In order to account for the incoming boundary layer profile, upstream flow properties are mass averaged of the cross section height. The equations of mass, momentum, energy conservation and the isentropic relation are applied to a control volume, which contains the pseudo-shock. By means of this model the flow conditions downstream of the pseudo-shock can be derived solely from the upstream mass averaged flow values but it is not possible to determine the flow characteristics inside the pseudo-shock. The static and total pressure ratios are given by Eqs. 9 and 10, respectively.

$$\frac{p_2}{p_1} = \frac{1 + \gamma\,(\xi_1/\sigma_1)\,\bar{\mathrm{Ma}}_1^2}{1 + \gamma\,\mathrm{Ma}_2^2} \tag{9}$$

$$\frac{p_{02}}{p_{01e}} = \left[\frac{2 + (\gamma - 1)\mathrm{Ma}_2^2}{2 + (\gamma - 1)\mathrm{Ma}_{1e}^2}\right]\frac{p_2}{p_1} \tag{10}$$

with

$$\bar{\mathrm{Ma}}_1 = \frac{\bar{u}_1}{\bar{a}_1} \quad \bar{u}_1 \equiv \left(\frac{\int \rho_1 u_1^3 \mathrm{d}A}{\int \rho_1 u_1\,\mathrm{d}A}\right)^{1/2} \bar{a}_1 \equiv \left(\frac{\int a_1^2 \rho_1 u_1 \mathrm{d}A}{\int \rho_1 u_1\,\mathrm{d}A}\right)^{1/2}$$

$$\sigma_1 \equiv \frac{\bar{\rho}_1\,\bar{u}_1}{\int \rho_1\,u_1\,\mathrm{d}A} \text{ and } \xi_1 \equiv \frac{\rho_1 u_1^2}{\bar{u}\int \rho_1\,u_1\,\mathrm{d}A}$$

These equations are applicable to flows in cylindrical ducts and rectangular ducts with semi-infinite span. In order to analyze the current flow problem with this model, the hydraulic diameter of the nozzle has been used, because the actual geometry is better approximated by a circular shape then a rectangular duct with semi-infinite span. A comprehensive presentation of the mass averaging pseudo-shock model can be found in Matsuo and Miyazato (1999).

The models cited here are not intended to be a comprehensive overview of all shock train models. Only, the most cited and applied ones are reviewed.

3 Results

In Fig. 6, theoretical and measured wall pressure plots of the primary nozzle are shown. The first plot shows the wall pressure as measured including the pressure rise induced by the shock train. The second plot has been added in order to illustrate the pressure rise that would occur if the supersonic flow is compressed not by a shock train but a single normal shock downstream of which the flow decelerates further due to the increasing area ratio. The Mach number of this single normal shock is determined with experimental values. Thirdly, the theoretical

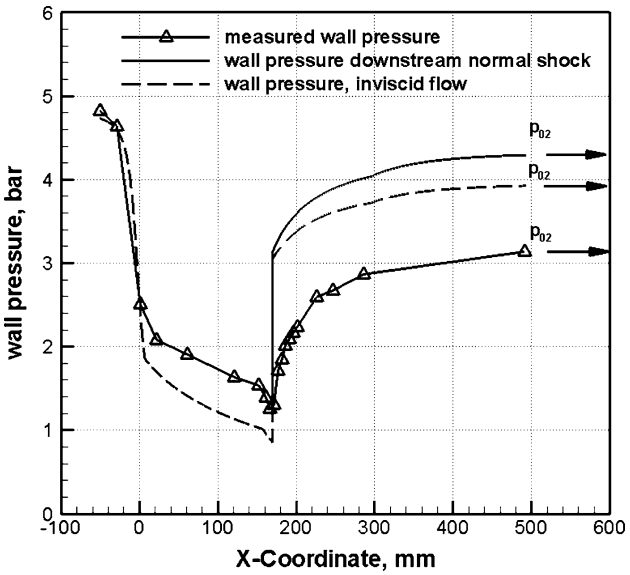

Fig. 6 Comparison between measurement and theoretical values, $p_{01} = 4.8$ bar, $T_0 = 293$ K

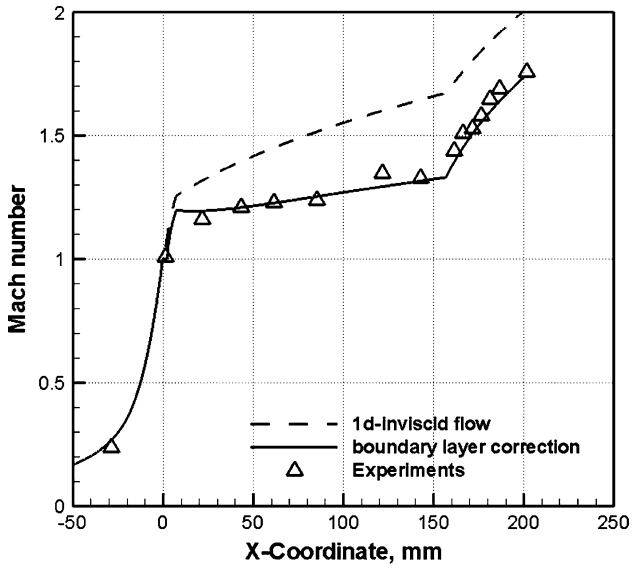

Fig. 7 Mach number plot along the first nozzle

wall pressure is shown, which is computed from the geometrical nozzle area ratio and therefore does not take into account any boundary layer effects. Also, in this case, it is assumed that the flow is compressed by a single normal shock.

The pressure rise across the normal shock is computed with the local ideal free stream Mach number and the normal shock relation. In all cases downstream of the compression region the pressure continues to rise that is because the nozzle walls diverge. Therefore, the nozzle acts like a subsonic diffusor. Comparing the three pressure distributions in Fig. 6, it becomes obvious that due to viscous effects in the mixing region but mostly because of the structure of the shock train i.e. a series of nearly normal shocks, the total pressure loss is considerably higher than for a single normal shock.

The deviance between the ideal 1d, inviscid pressure distribution, and the actual measurements is illustrated more clearly in Fig. 7. Three Mach number plots are depicted for the undisturbed supersonic flow upstream of the shock system. The experimental Mach number has been deduced from the static wall pressure measurements and the total pressure in the settling chamber. By comparison, the dashed line shows the Mach number distribution based on the geometric area ratio of the nozzle. The deviation is quite significant. Obviously, the growing boundary layer reduces the effective area ratio; therefore the gas flow does not expand that strongly.

In order to resolve the shortcoming of the quasi 1d-model, the boundary layer thickness 170 mm downstream of the nozzle throat was measured with the total pressure probe described previously. The velocity profiles deduced from the pressure profiles measured in the horizontal and vertical plane of the channel are shown in Fig. 8. Because the probe represents a blunt body in a supersonic flow a normal shock establishes in front. In this case the local, upstream Mach number needs to be determined iteratively by the Pitot-Rayleigh equation for normal shocks. For this, the density profile across the boundary layer is approximated by the assumption of a constant total temperature, which is measured in the settling chamber upstream of the first nozzle. In flow direction, the total temperature is considered constant because the gas is nonreactive, and the heat flow across the nozzle wall due to the temperature gradient is rather small. The total temperature of the flow and wall temperature are approximately at ambient temperature. Because of the negligible heat transfer across the wall, the total temperature change across the boundary layer is also negligible (Shapiro 1954).

From the velocity profile, the displacement thickness of the boundary layer has been determined with $\delta_1^*(x = 170\text{ mm}) = 0.27$ mm in the vertical plane and $\delta_2^*(x = 170\text{ mm}) = 0.44$ mm in the horizontal plane. Assuming a turbulent boundary layer the boundary layer displacement thickness is correlated with the distance between the nozzle throat and the measuring point. According to common boundary layer theory, the growth of the displacement thickness of a turbulent boundary layer correlates with the length of the wetted surface to the power of 0.8 (Schlichting 1997). Hence the displacement thickness of the undisturbed boundary layer along the channel walls is approximated by

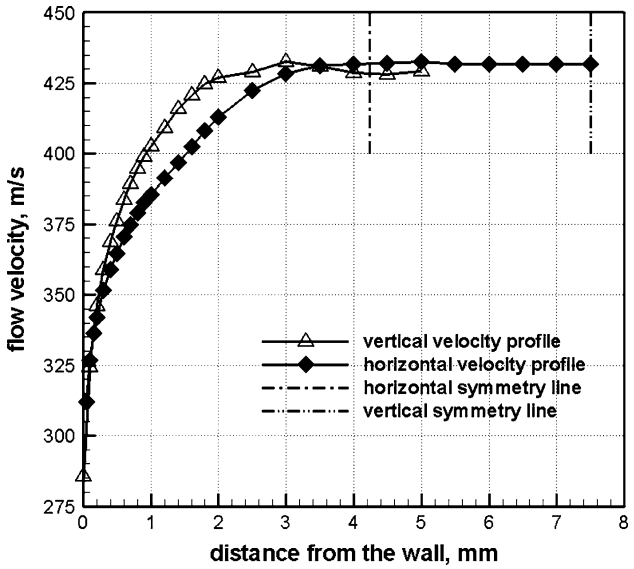

Fig. 8 Horizontal and vertical boundary layer profile

$$\delta_1^* = 0.27\,\mathrm{mm}\left(\frac{x}{170\,\mathrm{mm}}\right)^{0.8} \quad \text{upper wall} \tag{11}$$

$$\delta_2^* = 0.44\,\mathrm{mm}\left(\frac{x}{170\,\mathrm{mm}}\right)^{0.8} \quad \text{side wall} \tag{12}$$

Similarly, the momentum displacement thickness of the upstream boundary layer have been approximated by

$$\theta_1 = 0.24\,\mathrm{mm}\left(\frac{x}{170\,\mathrm{mm}}\right)^{0.8} \quad \text{upper wall} \tag{13}$$

$$\theta_2 = 0.38\,\mathrm{mm}\left(\frac{x}{170\,\mathrm{mm}}\right)^{0.8} \quad \text{side wall} \tag{14}$$

As depicted in Fig. 7 if the displacement thickness is taken into account to determine the effective area ratio, the computed and measured Mach numbers agree very well, even though Eqs. 11 and 12 are strictly valid only for boundary layers over a flat plate.

The good agreement indicates that the weak pressure gradient along the supersonic part of the nozzle is not sufficiently strong to have a distinct effect on the boundary layer growth. Figures 9a, b show the computed and measured wall pressure contours in the shock train. Of the four different models applied the empirical model from Billig (1992) for square ducts agrees best with the measured values for the first part of the shock train. The model is applied twice, firstly by using the boundary layer momentum thickness of the upper wall and secondly by using the boundary layer momentum thickness on the side wall. As shown in Fig. 9a, the pressure plot that takes into account the upper wall boundary layer coincides very well with the measured wall pressure up to 210 mm. The authors believe that this observation can be explained by the fact that up to this distinct position along the nozzle

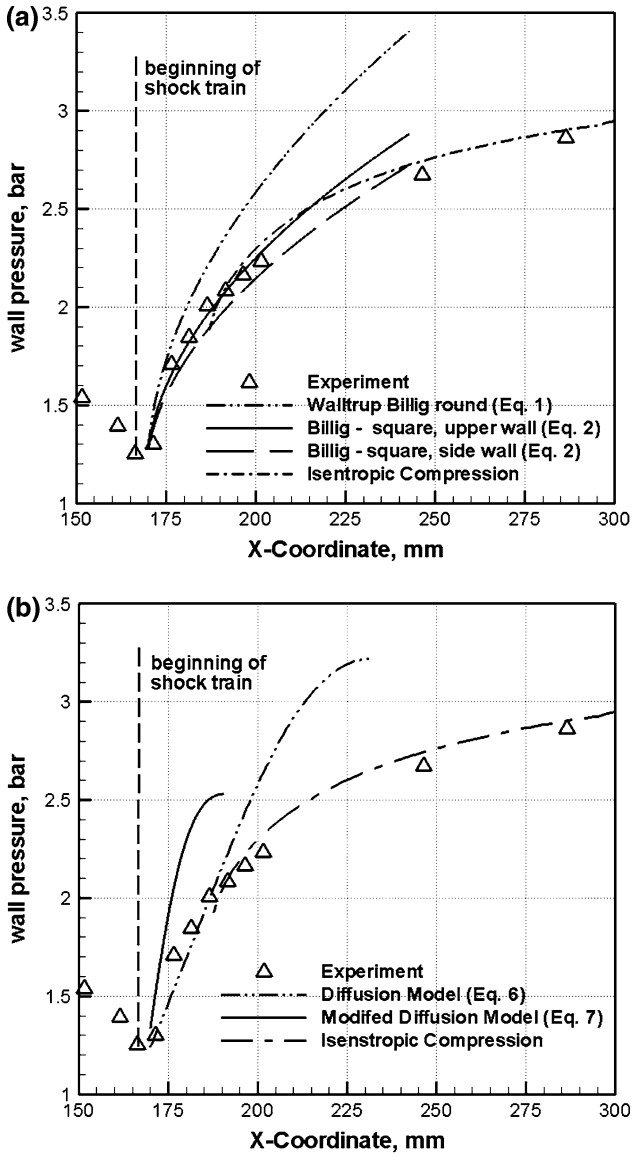

Fig. 9 Measured and computed pressure rise along the shock train, Ma = 1.5, $Re_x = 12.9 \times 10^6$, $x = 170$ mm

axis the height of the channel is only about half its width. Therefore, the boundary layer on the upper wall has a stronger effect on the pressure distribution than the side wall boundary layers.

The results of the diffusion and modified diffusion model are summarized in Fig. 9b. However, these models significantly overpredict the pressure gradient. Interestingly, if the conditions in the downstream settling chamber are chosen as reference values for an isentropic flow, the thus computed pressure only changes due to the local area ratio and follows the experimental wall pressure fairly well from $x = 190$ mm. This plot is termed isentropic compression in Fig. 9a, b. The remaining deviation can be attributed to viscous effects and shock losses.

The shock-less model and the mass averaging model are not capable to resolve the pressure distribution along the shock train but the pressure ratio across the entire pseudo-shock region. Therefore, in Table 1 results of these two shock models and of the diffusion models concerning the total pressure ratio across the shock train are summarized for the flow conditions stated in Fig. 9.

Table 1 Shock train length and total pressure ratio, $Ma_1 = 1.5$

Model	Total pressure ratio p_{02}/p_{01}
Normal shock	0.93
Experiment	0.68
Mass averaging model	0.66
Diff. model	0.67
Mod. diff. model	0.47
Shock-less model	0.93

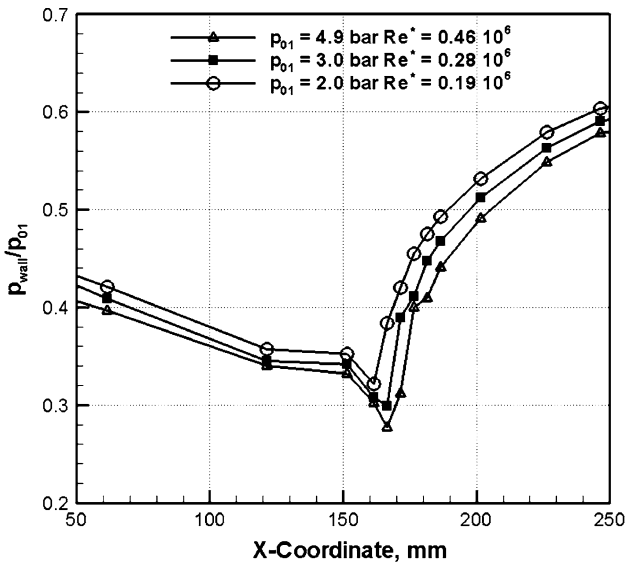

Fig. 10 Normalized wall pressure

The mass averaging model and the diffusion model perform best, predicting the total pressure downstream of the shock train very accurately. The shock-less model on the other hand significantly overestimates the pressure increase. The bad performance of this model has also been observed by others (Ikui et al. 1980; NAVWEPS 1959).

Since the mass averaging model is capable to compute the total pressure ratio across a shock train and the empirical model from Billig performs best in predicting the pressure rise along the shock train, those models appear to be suitable to compute a shock train only from the upstream flow parameter.

Figure 10 shows experimental results for different total pressures values. The cross section areas of the first and second nozzle are unchanged in all three cases.

As the total pressure is reduced the throat Reynolds numbers drops and the boundary layer becomes thicker, which leads to an increased confinement level hence lesser expansion and a smaller free stream Mach number. Because of the limited variation of the Reynolds number the wall pressure measurements do not indicate a significant relocation of the onset of the shock train. On the Schlieren images in Fig. 11, it can be observed that the location of the compression region as well as the visible length of the shock train does change. Over the range of the pressure variation, the shock train shifts about 8 mm closer toward the nozzle throat. Because of the current geometry of the nozzle, the free stream Mach number cannot be kept constant but changes with the boundary layer thickness and the associated axial position of the first shock. Therefore, in this case, it is not possible to make a clear distinction between the influence of the Reynolds number i.e. boundary layer thickness, and the free stream Mach number on the shock train position and length.

The influence of solely the Mach number onto the shock train length is depicted in the following images in Fig. 12. For the variation of the Mach number, the total pressure is kept constant but the area ratio between the primary and secondary nozzle has been changed, which leads to a

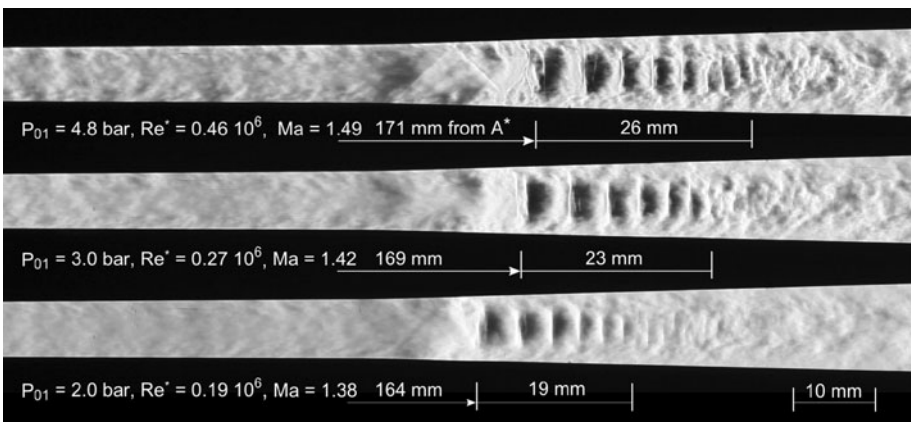

Fig. 11 Shock position at different Reynolds and Mach numbers

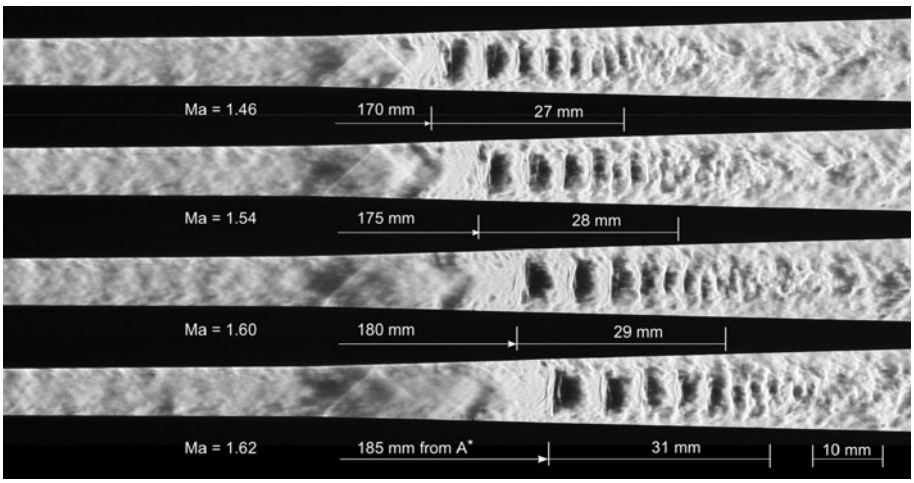

Fig. 12 Influence of shock Mach number on shock train position and length $p_{01} = 4.8$ bar, $Re^* = 0.46 \times 10^6$

different back pressure. As the Mach number changes from 1.46 to 1.62 the shock train becomes longer, and the turbulent mixing is much stronger. For the sake of correctness one must note that due to the relocation of the shock train the Reynolds number Re_θ also changes.

However, the Reynolds number Re_θ changes only in the order of 1% and the empirical Eqs. 1 and 2 quoted earlier also show that the Reynolds number correlates with an exponent of 0.2 and 0.25 compared to the Mach number, which changes by the power of two. Therefore, in this case the Reynolds number effect is deemed negligible. In order to evaluate the performance of the empirical model of Billig and the mass averaging model, the pressure ratio across the shock train has been recomputed for different Mach numbers. The results are shown in Fig. 13 and Table 2. Because the displacement thickness of the upstream boundary layer is unknown, it was approximated from Eq. 13.

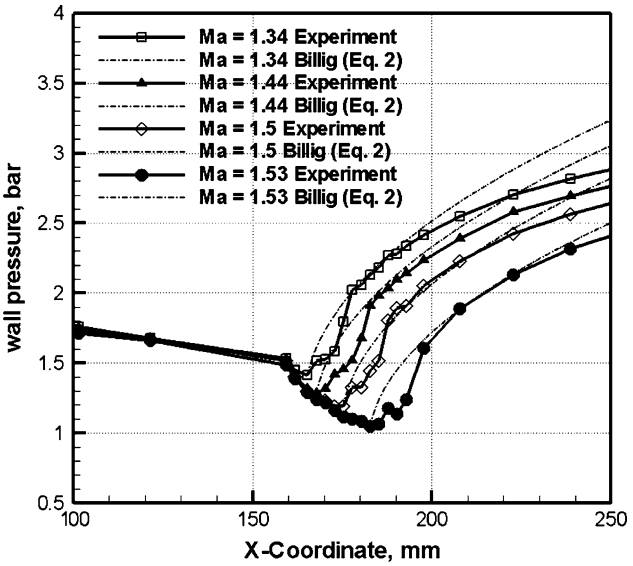

Fig. 13 Comparison of measured and computed wall pressure, $Re^* = 0.46 \times 10^6$

Table 2 Comparison between measured and computed back pressure, $p_{01} = 4.8$ bar

Mach number	Back pressure p_{02} [bar] experiment	Back pressure p_{02} [bar] mass averaging model
1.34	3.28	3.4
1.44	3.19	3.29
1.5	3.17	3.12
1.53	3.05	3.02

As shown in Fig. 13, the empirical model from Billig reproduces the pressure gradient reasonably well in particular in the shock train region. Downstream of which in the mixing region, the computed pressure is larger compared to the measured pressure. The reason that the within the shock train region measured pressure values do not steadily increase is likely to be flow separation at the beginning of the shock train.

The deviations between measurements and the theoretical data can be explained by the fact that the empirical model of Billig does not take into account the pressure recovery by the mixing region. Furthermore, difficulties arise in determining the lowest wall pressure value hence the actual onset of the shock train, which is required as input data for the empirical model. Also, the local boundary layer displacement thickness, a likewise important parameter in the model, has been determined with some uncertainty.

In contrast to the model of Billig, which does not yield a defined back pressure or shock train length the mass averaging model performs well in reproducing the total pressure downstream of the pseudo-shock. (see Table 2).

Because the pressure increase downstream of the pseudo-shock can be approximated with the isentropic equation, the following procedure can be applied to calculate the pressure increase across the entire pseudo-shock system. Firstly, the pressure rise in the shock train region is

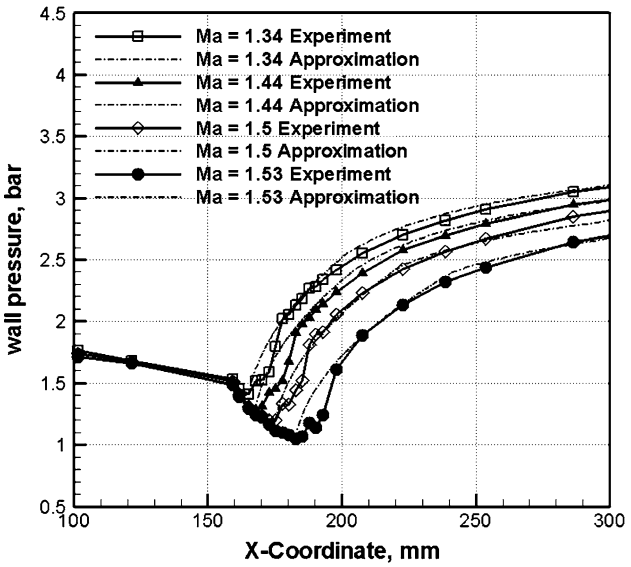

Fig. 14 Combined pressure plots of Billig and mass averaging shock train model compared with experiment

derived from the empirical model of Billig. Secondly, the total pressure in the downstream settling chamber is computed with the mass averaging model. By applying the isentropic equation and taking into account the changing cross section area, a second pressure plot describing the changing pressure downstream of the shock train is obtained. Both pressure curves intersect eventually, and the overall pressure distribution is obtained. As depicted in Fig. 14 in the present case only the flow conditions upstream of the shock and the geometry of the wind tunnel need be known to compute the pressure distribution along the pseudo-shock with good accuracy.

4 Conclusions

A literature review shows that quite a number of different shock train models have been brought forward over time. It was found that for the shock train in a narrow rectangular channel at moderate Mach numbers the empirical model for square ducts of Billig reproduces the pressure rise best. The total pressure loss across the shock train is well predicted by the mass averaging model. A procedure was presented, which combines both models and allows to derive the pressure change across the pseudo-shock system solely from upstream flow conditions and wind tunnel geometry.

This work is intended as analysis of the pseudo-shock flow phenomenon. In a next step, the shock boundary layer interaction is going to be manipulated by suction or blowing in order to improve the pressure recovery across the shock train.

Acknowledgments The research reported in this paper was funded by the DFG (German research foundation) PAK 75/1 'A new gas dynamic process for the production of nanoparticles'. Thanks to Thomas Gawehn from the DLR Cologne and Nisar Al-Hasan from the Technical University Munich for many fruitful discussions.

References

Bement DA, Stevens JR, Thompson MW (1990) Measured operating characteristics of a rectangular combustor/insolator, AIAA Paper No.90-2221

Billig F (1992) Research on supersonic combustion. J Propuls Power 9(4):499–514

Carroll BF (1990) Characteristics of multiple shock wave/turbulent boundary-layer interactions in rectangular ducts. J Propuls Power 6(2):186–193

Carroll BF, Lopez-Fernandez PA, Dutton JC (1993) Computations and experiments for a multiple normal shock/boundary-layer interaction. J Propuls Power 9(3):405–411

Crocco L (1958) One-dimensional treatment of steady gas dynamics In: Fundamentals of gas dynamics, ed. Emmons HW, Princeton University Press, pp 110–130

Cuffel RF, Back LH (1976) Flow and heat transfer measurements in a pseudo-shock region with surface cooling. AIAA J 14(12):1716–1722

Grzona A, Weiß A, et al. (2007) Gas-phase synthesis of non-agglomerated nanoparticles by fast gasdynamic heating and cooling, Proceeding of 26th international symposium on shock waves, Göttingen, Germany

Ikui T, Matsuo K, Nagai M (1974) The mechanism of pseudo-shock waves. Bull Jpn Soc Mech Eng 17(108):731–739

Ikui T, Matsuo K, Mochizuki H, Som K (1980) Pseudo-shock waves in a divergent channel. Bull JSME 23(175):20–25

Ikui T, Matsuo K, Sasaguchi K (1981) Modified diffusion model of pseudo-shock waves considering upstream boundary layer. Bull Jpn Soc Mech Eng 24(197):1920–1927

Lukasiewicz J (1953) Diffusers for supersonic wind tunnels. J Aeronaut Sci 20:617–626

Matsuo K, Miyazato Y (1999) Mass averaging pseudo-shock model in a straight flow passage. Proc Inst Mech Eng 213(6):365–375

Matsuo K, Mochizuki H, Miyazato Y (1990) An application of passive boundary layer control to pseudo-shock waves, Proceedings of 2nd KSME-JSME fluids engineering conference, Korea

Matsuo K, Miyazato Y, Kim HD (1999) Shock train and pseudo-shock phenomena in internal gas flows. Prog Aerosp Sci 35:33–100

NAVWEPS (1959) Handbook of Supersonic Aerodynamics, Vol. 6, No. 17, Ducts, Nozzles and Diffusers, p 271

Neumann EP, Lustwerk F (1949) Supersonic diffusers for wind tunnels. J Appl Mech 16:195–202

Nill LD, Mattick AT (1996) An experimental study of shock structure in a normal shock train, AIAA Paper No. 96-0799

Om D, Childs ME, Viegas JR (1985a) An experimental investigation and numerical prediction of a transonic normal shock/boundary layer interaction. AIAA J 23(5):707–714

Om D, Viegast JR, Childs ME (1985b) Transonic shock-wave/turbulent boundary layer interaction in a circular duct. AIAA J 23(5):707–714

Schlichting H (1997) Grenzschicht-theorie. Springer, Berlin

Shapiro AH (1954) The dynamics and thermodynamics of compressible fluid flow. The Ronald Press Company, New York

Squire LC (1996) Interaction of swept and unswept normal shock waves with boundary layers. AIAA J 34(10):2099–2101

Waltrup PJ, Billig FS (1973) Structure of shock waves in cylindrical ducts. AIAA J 11(10):1404–1408